Applied Surface Science 537 (2021) 147984

Contents lists available at ScienceDirect

Applied Surface Science

journal homepage: www.elsevier.com/locate/apsusc

Quantification of surface contamination on optical glass via sensitivity-improved calibration-free laser-induced breakdown spectroscopy

Christoph Gerhard[a,*], Aya Taleb[b,c], Frédéric Pelascini[c], Jörg Hermann[b]

[a] University of Applied Sciences and Arts, Faculty of Engineering and Health, 37085 Göttingen, Germany
[b] Aix-Marseille University, CNRS, LP3, 13009 Marseille, France
[c] Cetim Grand Est, 67400 Illkirch-Graffenstaden, France

ARTICLE INFO

Keywords:
Surface contamination
Trace elements
Calibration-free laser-induced breakdown spectroscopy
Glass surfaces
Optics manufacturing
Polishing

ABSTRACT

We report quantitative analysis of manufacturing-induced trace contaminants of optical glass surfaces by laser-induced breakdown spectroscopy (LIBS). Therefore, spectra recorded with an echelle spectrometer coupled to a gated detector were analysed using a calibration-free LIBS approach based on the calculation of the spectral radiance of a plasma in local thermodynamic equilibrium. The measurements were carried out in experimental conditions that enable both accurate modelling of plasma emission and high sensitivity for trace element analysis. Depth-resolved measurements were performed by recording spectra for successive laser pulses applied to the same irradiation sites. Validated via inductively coupled plasma atomic emission spectroscopy for the bulk glass composition, the measurements evidence a surface contamination that originates from polishing during glass manufacturing. The measured penetration depths of the contaminants are discussed in the frame of the underlying mechanisms of surface contamination and related to the changes of the optical properties evidenced by ellipsometric measurements. Demonstrated here for optical glass, the sensitivity-improved calibration-free LIBS approach can be used to quantify contaminations of surfaces in all kind of technological applications.

1. Introduction

In classical optics manufacturing polishing is achieved by different interactions of the glass surface with the used polishing pad material and the polishing suspension. The effect of surface smoothing is not yet fully understood, but generally based on four different mechanisms, (i) flow of glass material, (ii) fretting due to friction of the glass surface and the tool, (iii) mechanical removal via abrasion, and (iv) decomposition of the glass surface by chemical reactions [1]. Since the last two effects are typically predominant, the polishing process is usually referred to as chemo-mechanical polishing [2]. Mechanical removal can easily be described by the interaction of the glass surface with grains such as cerium oxide or aluminium oxide from the aqueous polishing slurry. Moreover, chemical reactions are induced by the polishing suspension. Here, the main mechanism is the penetration of water into the glass surface and an accompanying hydrolytic scission of the glass network [3]. By the following reaction of hydrogen and the constituents of the network forming silicon dioxide, a thin layer consisting of hydrated silica or silanol (Si-O-H) is formed [4,5]. This layer, referred to as polishing re-deposition layer or *Beilby* layer [6], has a thickness of some nanometres to some tens of nanometres [7,8]. In the course of layer growth, residues from polishing agents are usually embedded in the formed *Beilby* layer [6,9]. In addition, polishing agents and other elements from the polishing suspension can penetrate into the glass material due to hydrolysis and diffusion [10]. The penetration depth depends on the polishing agents, glass type and process parameters, and values up to several microns have been reported in literature [11].

This surface contamination may deteriorate the functionality of optics surfaces. For instance, it is well known that the presence of residues from polishing agents leads to a decrease of the laser damage threshold [12–14]. The damage threshold lowering is particularly severe for ultraviolet laser radiation due to the strong UV absorption of conventional polishing agents [15]. Further, such contaminants may also alter the near-surface index of refraction as shown in previous work [16]. As a result of a change in chemical composition at the glass surface, the index of refraction may notably differ from the nominal value of the bulk material, and the performance of a present dielectric functional coating may be lowered.

Against this background, laser-induced breakdown spectroscopy is proposed to investigate the polishing-induced surface contamination of heavy flint glass. LIBS was already used for analysis of glass, for example for quality control in industrial production [17], recycling

* Corresponding author.
E-mail address: christoph.gerhard@hawk.de (C. Gerhard).

https://doi.org/10.1016/j.apsusc.2020.147984
Received 14 July 2020; Received in revised form 27 August 2020; Accepted 23 September 2020
Available online 28 September 2020

[18,19], conservation of artworks [20–22], archaeometry [23], forensic research [24–26], and nuclear waste management [27–29]. Calibration-free laser-induced breakdown spectroscopy was shown to be a promising technique for quantitative analysis of complex multi-component glasses [30]. More recently, it was shown that calibration-free LIBS measurements enable the charcaterisation of multi-elemental thin films with analytical performances better than the traditional techniques of thin film analysis [31]. In the present work, we apply a sensitivity-improved calibration-free LIBS approach that was previously prosed to quantify trace-element contamination in seafood [32]. The method is here applied to perform accurate analysis of optical glass including depth-resolved measurements of major, minor, and trace elements.

2. Materials and methods

2.1. Sample preparation and initial characterisation

For the investigation of polishing-induced surface contamination plane parallel plates made of heavy flint glass (Schott, N-SF5) were produced by classical optics manufacturing. The plates were cut from a glass block using a water-cooled circular saw with a saw blade coated with a copper matrix and embedded diamond grains. The cut surfaces were then lapped using a slurry consisting of water and silicon carbide abrasive grains with different grain sizes. Starting with rough lapping, the grain size was successively reduced. After fine lapping, the samples were polished for 6 h on a polishing pad made of a polyurethane foil using a cerium oxide-based polishing suspension (Pieplow & Brandt, Ceri3000). In the course of all manufacturing steps, tap water was used for mixing the aqueous cooling lubricant, the lapping slurry, and for thinning down the polishing suspension. After polishing, the index of refraction of the polished surfaces was measured using an ellipsometer (Accurion, model ep4) at a wavelength of 546.1 nm.

Heavy flint glass was chosen as sample material since this type of glass has a notable relevance in optics manufacturing. Due to its high index of refraction and low V-number it is an essential medium for the realisation of optical systems with high imaging quality. In combination with crown glasses it allows for the minimisation of chromatic aberrations. Heavy flint glasses are further used in spectacle optics in order to produce thin ophthalmic lenses with high optical refraction power. Since flint glass features a considerable nonlinear behaviour and a significantly higher peak Raman gain than fused silica it is also used for the production of photonic crystal fibres for supercontinuum generation [33,34]. However, the impact of optics manufacturing and especially polishing on the chemical composition of polished heavy flint glass surfaces is usually not considered in literature whereas extensive work was reported for fused silica, see summary in [11].

2.2. Calibration-free LIBS measurements

The LIBS experiment is illustrated by the scheme in Fig. 1(a). The plasma was generated on the heavy flint glass sample surfaces using Nd:YAG laser (Quantel, model Brilliant) pulses of 4 ns duration. The laser was operated at its fourth harmonic wavelength of 266 nm. The laser pulse energy was attenuated down to 6 mJ using an energy control unit consisting of a half-wave plate and a polariser. The laser beam was focussed onto the sample surface by a plano-convex lens with a focal length of 150 mm. According to a beam diameter of 100 µm on the sample surface, the incident laser fluence was of about 100 J/cm^2. This fluence was shown to be large enough to ensure stoichiometric ablation [35]. The samples were placed on a motorised xyz linear stage mounted in a vacuum chamber of 10^{-4} Pa residual pressure. During LIBS measurements, the chamber was filled with argon at a pressure of 5×10^4 Pa. We emphasise that the precise pressure has no influence on the analytical performance of the method and that the measurements can be performed with an argon jet in ambient air for practical reasons.

The emission of the laser-produced plasma was captured by a condenser setup consisting of two convex lenses with focal lengths of 150 mm and 35 mm, respectively, and coupled into a multimode optical fibre of 600 µm core diameter. According to an image magnification of about 1:5, a cylindrical volume of 3 mm diameter was observed to make sure that emission from the entire plasma was captured. The optical axis of observation was tilted by an angle of 15° with respect to the surface normal. The optical fibre was coupled to an echelle spectrometer (LTB, model Aryelle Butterfly) with a resolving power of 1×10^4. The spectrometer was equipped with an intensified charge-coupled device (ICCD) matrix detector (Andor, model IStar) for time-resolved spectra recordings.

The measured spectra were analysed using a calibration-free LIBS measurement procedure based on the calculation of the spectral radiance of the laser-induced plasma. To enable accurate modelling of the plasma emission, the experimental conditions were chosen so that the plasma is in local thermodynamic equilibrium and characterised by almost uniform spatial distributions of temperature and densities [36]. In that condition, the emission spectrum of a plasma composed of n elements is determined by $n + 2$ parameters, the temperature T, the electron density n_e, the relative fractions of n-1 elements, and the plasma diameter along the line of sight L [30]. An iterative algorithm is used to deduce the parameters from the comparison of the measured and computed spectra in the spectral ranges of appropriate spectral lines. The algorithm consists of principal loop for the successive measurements of the $n + 2$ parameters with an embedded calculation loop for the derivation of each parameter from the best agreement between measured and computed spectra in the ranges of preselected spectral lines [see Fig. 1(b)].

Calibration-free LIBS measurements usually suffer low sensitivity. To satisfy the condition of local thermodynamic equilibrium (LTE), the electron density must be large enough so that the rates of collisional excitation and de-excitation dominate the radiative decay [37]. The processes of bremsstrahlung and radiative recombination associated to the charged particles generate a continuum radiation that hinders the observation of low-intensity spectral line emission from trace elements. To increase the sensitivity of the calibration-free LIBS measurements, we apply a two-step procedure that was recently proposed for trace-element analysis of organic materials [32]. The method is based on the recording of two spectra with different delays between the laser pulse and the detector gate. The early measurement is performed in full LTE conditions, when the electron density is large enough to ensure Boltzmann equilibrium distributions of all plasma species. According to the low signal-to-noise ratio, this spectrum enables the quantification of major and minor elements only. To complete the analysis, a second spectrum is recorded with larger delay. Due to the lower electron density, the equilibrium condition is not fulfilled for all elements. Atoms such as oxygen, characterised by large energy gaps between their electronic excitation levels, are out of equilibrium. Contrarily, the equilibrium condition is still fulfilled for metallic atoms as their energy levels lie closer to each other. The number of charged particles being reduced, the continuum emission intensity is lower and low-intensity emission lines are observable with an improved signal-to-noise ratio. This situation is exploited to quantify trace elements. In the present experiment the early and late measurements were recorded with gate delays t_d of 400 ns and 2000 ns, respectively. The corresponding gate widths were set to $\Delta t_g = t_d/2$ to make sure that the variations of electron density n_e and temperature T during the time of observation are small compared to their absolute values. We measured $n_e = 3.2 \pm 0.8 \times 10^{17}$ cm^{-3} and $T = 13200 \pm 400$ K for the early delay, and $n_e = 4.1 \pm 1.1 \times 10^{16}$ cm^{-3} and $T = 8800 \pm 300$ K for the late delay.

Depth-resolved measurements were performed by recording spectra for consecutive laser pulses applied to single ablation sites. Each recording was obtained by accumulating the signal over 100 ablation sites to reach a sufficiently large signal-to-noise ratio. The depth of the

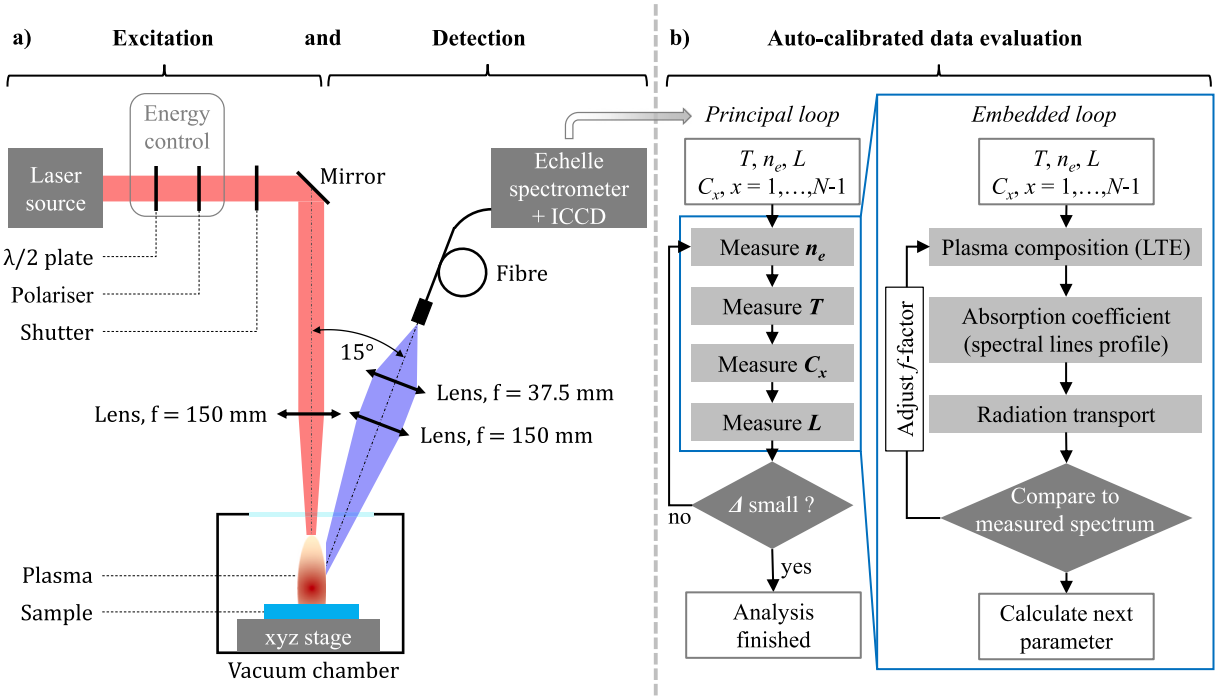

Fig. 1. (a) Experimental setup used for LIBS spectra recordings and (b) flow chart of the applied calibration-free LIBS measurement approach consisting of a principal loop for the consecutive measurements of electron density n_e, temperature T, elemental fractions C_x and plasma diameter L, and an embedded calculation loop for the determination of each single parameter.

Table 1
Transitions used for calibration-free LIBS measurements: wavelength λ, transition probability A_{ul} with relative error ΔA_{ul}, energy E and statistical weight g of lower (index l) and upper (index u) electronic states, Stark broadening width w and shift d for $n_e = 1 \times 10^{17}$ cm^{-3}.

Species	λ (nm) [reference]	A_{ul} (μs^{-1})	ΔA_{ul} (%)	E_l (eV)	g_l	E_u (eV)	g_u	w (pm)	d (pm)
Pb I	363.957 [40]	32.0	20	0.97	3	4.38	3	27	14
O I	777.194 [41]	36.9	7	9.15	5	10.74	7	105	15
Si I	390.552 [42]	13.3	15	1.91	1	5.08	3	31[a]	16[a]
K I	769.896 [43]	37.5	5	0.00	2	1.61	2	105	24
Na I	588.995 [44]	61.6	2	0.00	2	2.10	4	44	13
Ba II	455.403 [45]	111	15	0.00	2	2.72	4	40	−1.7
Ca II	393.366 [46]	140	25	0.00	2	3.15	4	20[b]	−4.0[b]
Al I	394.400 [47]	49.9	10	0.00	2	3.14	2	29	19
Zn I	481.053 [48]	70.0	25	4.08	5	6.65	3	64	38
La II	394.910 [49]	147	10	0.40	7	3.54	9	17	0.00
Mg I	517.268 [50]	33.7	10	2.71	3	5.11	3	90	50
Li I	670.776 [51]	36.9	1	0.00	2	1.85	4	39	−2.7
Ti II	336.121 [52]	158	25	0.03	8	3.72	10	11	0.06
Fe I	358.119 [53]	102	7	0.86	11	4.32	13	11	2.0
Ag I	328.068 [54]	140	5	0.00	2	3.78	4	16	0.00
Cu I	324.754 [55]	140	2	0.00	2	3.82	4	1.4[c]	0.00[c]
Sr II	421.552 [56]	126	7	0.00	2	2.94	2	41	−3.4

[a] Ref. [57].
[b] Ref. [58].
[c] Ref. [59].

laser-produced craters was measured via optical microscopy (Nikon, model Eclipse LV100ND). The spectral lines used for the quantification of major, minor, and trace elements are listed in Table 1 with the data used for the calculations. Most Stark broadening parameters have been measured in a separate experiment as illustrated in Refs. [38,39]. Although the applied calibration-free approach accounts for self-absorption, all measurements have been performed with lines of optical thickness < 1. We note that the resonance lines of potassium and sodium neutral atoms have moderate optical thickness during the early measurement when the major elements are quantified.

2.3. Inductively coupled plasma atomic emission spectroscopy

The depth-resolved calibration-free-LIBS measurements have been validated by comparing the composition deduced for the bulk glass to that obtained via inductively coupled plasma atomic emission spectroscopy (ICP-AES). Here, a commercial ICP-AES system (Varian, model Vista-MPX with axial aim) was used to measure the mass fractions of all elements. For this purpose, a sample with a mass of 100 g was taken from the investigated glass. The fractions of Si and La were determined by acid dissolution after alkaline melting (Spectroflux, high purity $Li_2B_4O_7$) whereas the other elements were measured in a solution obtained by fluoro-nitric acid etching. All reagents used were of analytical

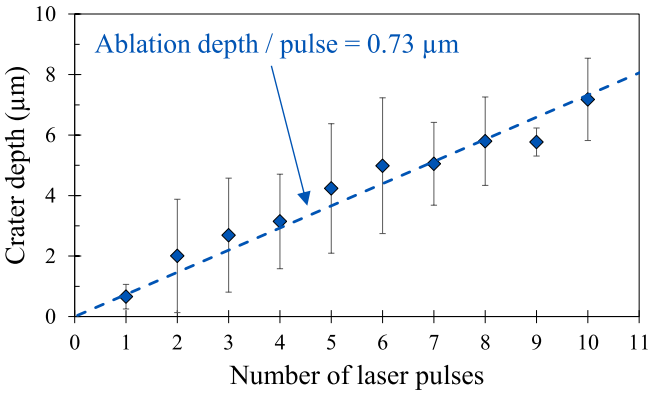

Fig. 2. Crater depth versus number of applied laser pulses.

grade.

3. Results and discussion

3.1. In-depth measurements of glass surfaces

Depth-resolved LIBS measurements require the knowledge of the ablation depth produced by each consecutive laser pulse. Therefore, a series of craters was drilled with an increasing number of laser pulses and the depth of the craters was measured via optical microscopy. From the linear growth of crater depth with the number of laser pulses observed in Fig. 2, an ablation depth of 0.73 µm per pulse is deduced. The variation in crater depth as represented by the error bars can be explained by the brittle character of the investigated glass and the resulting differences in material removal during phase explosion induced by the high applied fluence.

Cerium oxide-based polishing suspensions are usually a mixture of cerium oxide and lanthanum oxide [13]. For the commercial polishing suspension used in the present work the cerium oxide content is merely 60–65 wt% where the total content of rare earths is 86–91 wt% [60]. The second major constituent is lanthanum oxide and in some cases, the lanthanum content in cerium polishing agents even exceeds 30 wt% [61,62]. An amount of lanthanum comparable to that of cerium was also evidenced by the present LIBS measurements. Both elements are characterised by rich emission spectra composed of many atomic and ionic transitions. However, the most intense cerium lines are interfered with atomic or ionic transitions of other elements. Thus, the limit of cerium detection was of about one order of magnitude higher than that of lanthanum detection. The spectral line that was used to quantify lanthanum is observed in the spectrum shown in Fig. 3. The spectrum exhibits also several transitions that were used for the quantification of aluminium, barium and calcium.

The mass fraction of calcium deduced from the LIBS measurements is displayed in Fig. 4 as a function of depth. It is maximum at the sample surface and decreases exponentially to the constant value of the bulk glass. The description by an exponential decay represented by the solid line allows us to deduce mass fractions of 290 ppm and 45 ppm at the surface and for the bulk, respectively.

3.2. Validation via ICP-AES measurements

The measurement accuracy of the calibration-free LIBS analysis was evaluated by comparing the elemental fractions deduced for the bulk glass to reference values obtained via ICP-AES analysis (see Table 2). In addition, the elemental fractions are compared to values measured previously with a simple calibration-free approach based on single spectrum analysis [30].

Due to the lower sensitivity, the previous LIBS analysis enabled the quantification of a reduced number of elements only. The measured

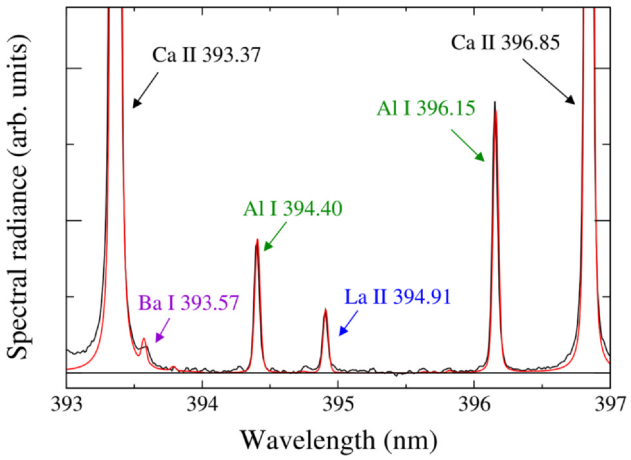

Fig. 3. Measured (black curve) and computed (red curve) spectral radiance of transition from calcium, barium, aluminium, and lanthanum. The spectrum was recorded with a gate delay of 2 µs and gate width of 1 µs. (For interpretation of the references to colour in this figure legend, the reader is referred to the web version of this article.)

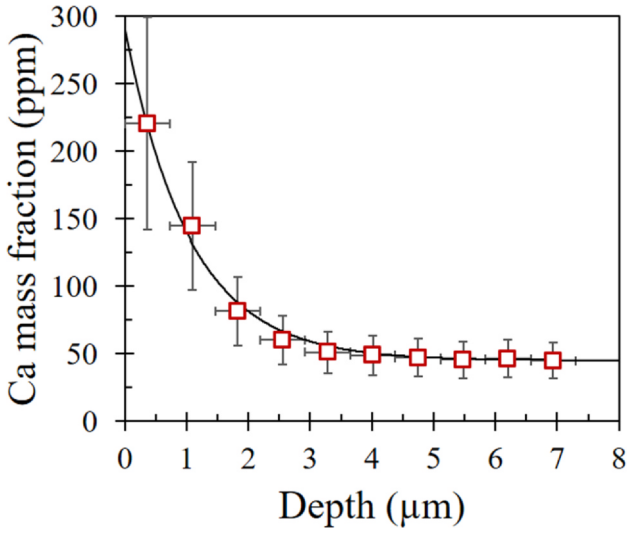

Fig. 4. Mass fraction of calcium in heavy flint glass versus depth.

mass fractions are in fair agreement with the reference values. The sensitivity-improved calibration-free LIBS approach enables the quantification of several trace elements that have not been quantified previously. The mass-fractions deduced for the bulk glass are in good agreement with the reference values for most elements. The main error sources are attributed to the accuracy of transition probabilities and to intensity measurement errors. The latter are due to low signal-to-noise ratio and/or uncertainties in the apparatus response correction.

3.3. Characterisation of surface contamination

The mass fractions of several trace elements measured via calibration-free LIBS are displayed in Fig. 5 as functions of depth. It is shown that silver and titanium (a) are uniformly distributed within the glass. Both elements are known trace contaminants in heavy flint glasses [63]. Contrarily, lanthanum (b) and magnesium (c) have non-uniform depth distributions. Similar to the distribution of calcium (see Fig. 4), their mass fractions have a maximum at the sample surface and decrease exponentially with increasing depth. The residual amount of magnesium is small within the bulk glass. Lanthanum is absent in the bulk indicating that this element originates from the surface polishing

Table 2
Mass fractions of the glass-composing elements measured via sensitivity-improved calibration-free LIBS for the surface $C_{LIBS,\ surface}$ and for the bulk $C_{LIBS,\ bulk}$ including comparison to values previously measured via calibration-free LIBS $C_{LIBS,\ 2014}$ and to reference values C_{ref} from ICP-AES analysis.

Element	Unit	$C_{LIBS,\ 2014}$	$C_{LIBS,\ surface}$	$C_{LIBS,\ bulk}$	C_{ref}
Si	%	19.6	18.7	18.7	18.04 ± 0.15
Ba		0.14	0.22	0.22	0.246 ± 0.003
K		2.96	4.4	4.4	3.50 ± 0.03
Na		1.18	1.5	1.5	1.21 ± 0.07
Pb		50.4	48.6	48.6	49.45 ± 0.92
Ti	ppm	–	16	16	13 ± 1
Al		–	200	100	68 ± 1
Ca		32	290	45	50 ± 2
Sr		–	3	1	1 ± 0.3
Mg		–	180	2	5.7 ± 0.3
Li		–	40	–	< 5[b]
La		–	220	–	< 2[b]
Fe		–	10	10	5 ± 2
Ag		–	6	6	4 ± 0.2
Cu		–	6	–	< 3[b]

[a]Ref. [30].
[b] Limit of quantification of ICP-AES measurement.

process only.

Neauport and co-workers [13] reported similar depth-dependence of La and Ce for cerium oxide-polished fused silica samples. They performed depth-resolved measurements by means of consecutive etching of 800 nm thick layers and ICP-AES analysis of the removed matter.

The enrichment of the near-surface region with calcium and magnesium is attributed to the use of tap water in the consecutive steps of sample preparation: (i) cutting, (ii) preparing the lapping slurry and (iii) thinning down the polishing suspension. The penetration depth derived from the exponential decrease is of 1.1 ± 0.2 µm and 1.0 ± 0.2 µm for lanthanum and calcium, respectively. The penetration depth of magnesium is notably higher and accounts for 1.8 ± 0.4 µm. This difference in penetration depth can be explained by the fact that magnesium is the smallest of those three elements and thus features the highest diffusion length. In addition to diffusion, elements transported by water can accumulate in the near-surface *Beilby* layer that is formed on the surface and within micro cracks during polishing of silicon dioxide-based glasses. Such accumulation of residues from polishing agents in this layer is quite well known in literature [6,9] and a similar depth-dependence as measured in this work was partially observed as already mentioned above [13].

It should finally be noted that the depth of penetration of residues from polishing suspensions strongly depends on the particular glass and the applied process parameters during polishing. For example, quite different values for cerium are reported in literature [11], ranging from 40 nm [64] up to 8 µm [65].

3.4. Impact of surface contamination on optical properties

As shown in the previous section, the near-surface glass layer is contaminated by trace elements originating from operating materials used in optics manufacturing. This leads to an alteration of the chemical composition of this layer up to a depth of several microns. Since the optical properties of any glass strongly depend on the glass stoichiometry and admixtures, the observed manufacturing-induced contamination results in a modification of optical parameters such as the index of refraction. This was verified by ellipsometric measurements of the polished heavy flint glass surfaces. As shown in Fig. 6, the actually measured index of refraction differs from the theoretical or nominal one as specified by the manufacturer's data sheet.

The measured index of refraction of 1.6747 is notably lower than the reference value of 1.6776 [66]. This can be explained by the

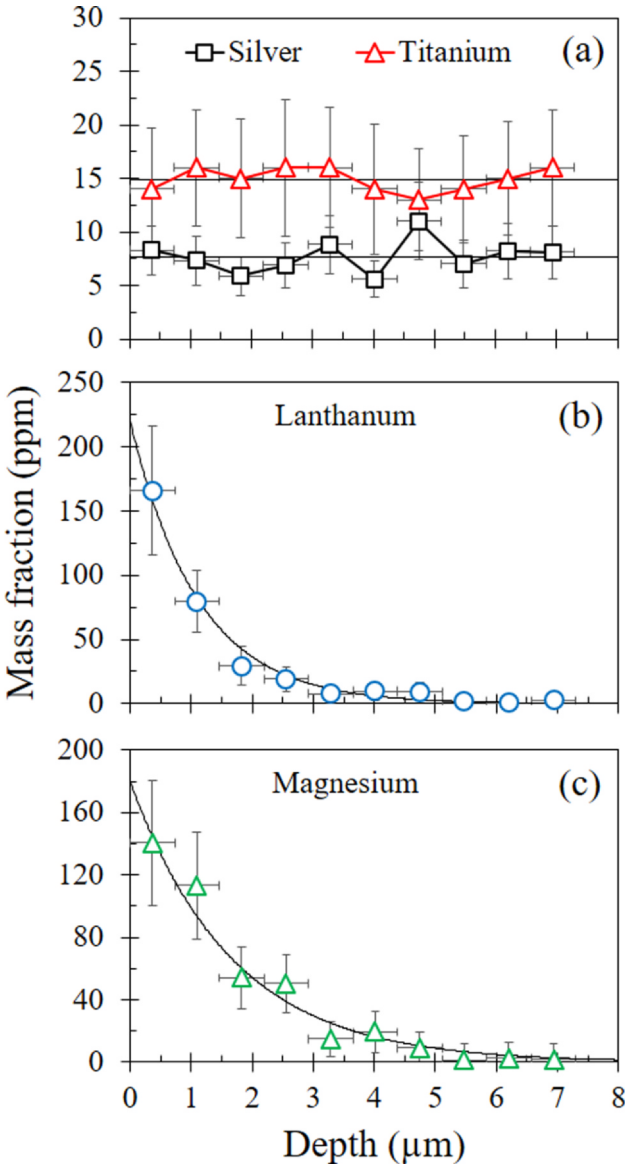

Fig. 5. Mass fractions of selected trace elements – silver and titanium (a) as well as lanthanum (b) and magnesium (c) – in heavy flint glass versus depth.

modification of the chemical composition in the near-surface region during the manufacturing process by means of the observed accumulation of contaminants. Even though the glass bulk material is not affected by the manufacturing process the change in index of refraction at the surface has an appreciable effect on the functionality of an optical component. This mainly applies to the reflectance of the glass surface. For perpendicular incidence of light, the reflectance of an interface between air (n = 1.0003) and undisturbed heavy flint glass (n = 1.6776) is 6.40% as calculated by the simplified Fresnel equation. Considering the observed reduction in index of refraction (n = 1.6747), the reflectance accounts for 6.36%. As a percentage, the difference between both values consequently amounts to 0.64%. The possible impact of such deviation in index of refraction and surface reflectance, respectively, on dielectric coatings applied to contaminated glass surfaces was already discussed in previous work [16]. Summing up it can be stated that manufacturing-induced surface contamination may lead to a reduced or even insufficient performance of optical coatings in some cases.

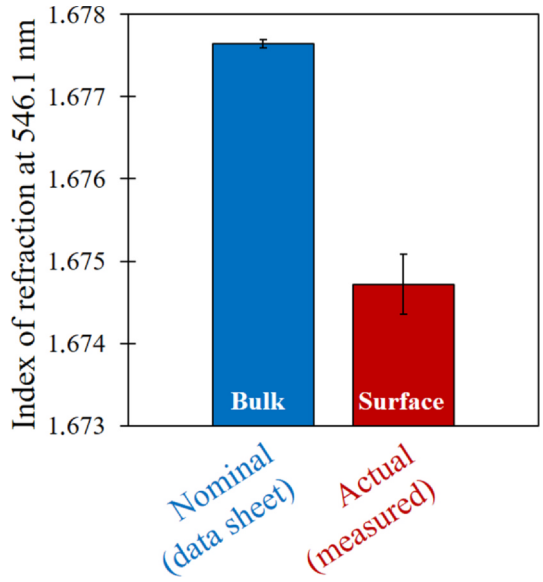

Fig. 6. Comparison of the nominal index of refraction of the investigated heavy flint glass bulk material to the actual index of refraction of the glass surface. The nominal value and its error bar were taken from the manufacturer's data sheet. The actual value was measured via ellipsometry where the error bar is given by the standard deviation of 25 single measurements.

4. Conclusions

We demonstrate that calibration-free LIBS is a powerful tool for accurate elemental analysis of materials with micrometric depth resolution. Using a sensitivity-improved calibration-free LIBS approach, we were able to measure the complex composition of heavy flint glass including major, minor and trace elements. The depth-resolved measurements allowed us to identify trace element contaminants according to the exponential decrease of their abundance from the surface into the bulk. The analytical performance of the method is illustrated by the comparison of the elemental fractions measured for the bulk glass to reference values obtained via ICP-AES analysis. The characterisation of the trace element contaminants via their mass fraction amounts and their penetration depths contributes to the better understanding of the interactions between glass surfaces, tools and working materials used in optics manufacturing. The findings are therefore useful to improve the manufacturing processes and consequently the performance of optical components. Validated here for analysis of multi-elemental heavy flint glass, the presented method is applicable to any materials that require accurate surface analysis in the view of their technological applications.

CRediT authorship contribution statement

Christoph Gerhard: Conceptualisation, Validation, Investigation, Resources, Writing - original draft, Writing - review & editing, Visualisation, Supervision, Project administration, Funding acquisition. **Aya Taleb:** Validation, Investigation, Writing - review & editing. **Frédéric Pelascini:** Validation, Investigation, Resources, Writing - review & editing. **Jörg Hermann:** Conceptualisation, Methodology, Software, Validation, Formal analysis, Investigation, Resources, Writing - review & editing, Visualisation, Supervision.

Declaration of Competing Interest

The authors declare that they have no known competing financial interests or personal relationships that could have appeared to influence the work reported in this paper.

Acknowledgements

The authors thank Lutz Müller and Daniel Tasche from the University of Applied Sciences and Arts for the preparation of the investigated samples and the help during experimentation. Special thank is also dedicated to Y. Ralchenko, A. Kramida, J. Reader, and the ASD Team at the National Institute of Standards and Technology, Gaithersburg, MD, for the free access to the NIST Atomic Spectra Database.

Funding

This project has received funding from the European Union's Horizon 2020 research and innovation programme under grant agreement No 654148 Laserlab-Europe (Project CNRS-LP3002491).

References

[1] C. Gerhard, Optics Manufacturing: Components and Systems, first ed., CRC Taylor & Francis, Boca Raton, 2017. https://doi.org/10.1201/9781351228367.
[2] R. Sabia, H.J. Stevens, Performance characterization of cerium oxide abrasives for chemical-mechanical polishing of glass, Mach. Sci. Technol. 4 (2000) 235–251, https://doi.org/10.1080/10940340008945708.
[3] L.M. Cook, Chemical processes in glass polishing, J. Non-Cryst. Solids 120 (1990) 152–171, https://doi.org/10.1016/0022-3093(90)90200-6.
[4] R.K. Iler, The Chemistry of silica: solubility, polymerization, colloid and surface properties and biochemistry of silica, first ed., Wiley Verlag, New York, 1979.
[5] M.J. Cumbo, S.D. Jacobs, Determination of near-surface forces in optical polishing using atomic force microscopy, Nanotechnology 5 (1994) 70–79, https://doi.org/10.1088/0957-4484/5/2/002.
[6] T. Suratwala, W. Steele, L. Wong, M.D. Feit, P.E. Miller, R. Dylla-Spears, N. Shen, R. Desjardin, Chemistry and formation of the Beilby layer during polishing of fused silica glass, J. Am. Ceram. Soc. 98 (2015) 2395–2402, https://doi.org/10.1111/jace.13659.
[7] L. Nevot, P. Croce, Characterization of surfaces by grazing X-ray reflection – application to the study of polishing of some silicate glasses, Rev. Phys. Appl. 15 (1980) 761–779.
[8] J. Trogolo, K. Rajan, Near surface modification of silica structure induced by chemical/mechanical polishing, J. Mater. Sci. 29 (1994) 4554–4558, https://doi.org/10.1007/BF00376278.
[9] J. Long, D. Ross, E. Tastepe, M. Lamb, Y. Funamoto, D. Shima, T. Kamimura, H. Yamaguchi, Fused silica contamination layer removal using magnetic field-assisted finishing, J. Am. Ceram. Soc. 103 (2020) 3008–3019, https://doi.org/10.1111/jace.17000.
[10] K. Kawagishi, H. Fukuyama, M. Susa, Aluminum diffusion in amorphous silica film, Proc. Symp. Intercon. Contact Metall. 31 (1997) 165–172.
[11] M. Pfiffer, J.-L. Longuet, C. Labrugère, E. Fargin, B. Bousquet, M. Dussauze, S. Lambert, P. Cormont, J. Neauport, Characterization of the polishing-induced contamination of fused silica optics, J. Am. Ceram. Soc. 100 (2017) 96–107, https://doi.org/10.1117/12.2244980.
[12] N.L. Boling, G. Dubé, Laser-induced inclusion damage at surfaces of transparent dielectrics, Appl. Phys. Lett. 23 (1973) 658–660, https://doi.org/10.1063/1.1654781.
[13] J. Neauport, L. Lamaignere, H. Bercegol, F. Pilon, J.-C. Birolleau, Polishing-induced contamination of fused silica optics and laser induced damage density at 351 nm, Opt. Express 13 (2005) 10163–10171, https://doi.org/10.1364/OPEX.13.010163.
[14] C. Gerhard, D. Tasche, N. Munser, H. Dyck, Increase in nanosecond laser-induced damage threshold of sapphire windows by means of direct dielectric barrier discharge plasma treatment, Opt. Lett. 42 (2017) 49–52, https://doi.org/10.1364/OL.42.000049.
[15] M.R. Kozlowski, J. Carr, I.D. Hutcheon, R.A. Torres, L.M. Sheehan, D.W. Camp, M. Yan, Depth profiling of polishing-induced contamination on fused silica surfaces, Proc. SPIE 3244 (1998) 365–375, https://doi.org/10.1117/12.307031.
[16] C. Gerhard, D. Tasche, O. Uteza, J. Hermann, Investigation of nonuniform surface properties of classically-manufactured fused silica windows, Appl. Opt. 56 (2017) 7427–7434, https://doi.org/10.1364/AO.56.007427.
[17] U. Panne, C. Haisch, M. Clara, R. Niessner, Analysis of glass and glassmelts during the vitrification process of fly and bottom ashes by laser-induced plasma spectroscopy. Part I: normalization and plasma diagnostics, Spectrochim. Acta B 53 (1998) 1957-1968. https://doi.org/10.1016/S0584-8547(98)00238-9.
[18] D.N. Stratis, K.L. Eland, S.M. Angel, Enhancement of aluminum, titanium, and iron in glass using pre-ablation spark dual-pulse LIBS, Appl. Spectrosc. 54 (2000) 1719–1726, https://doi.org/10.1366/0003702001948871.
[19] A.-M. Matiaske, I.B. Gornushkin, U. Panne, Double-pulse laser-induced breakdown spectroscopy for analysis of molten glass, Anal. Bioanal. Chem. 402 (2012) 2597–2606, https://doi.org/10.1007/s00216-011-5165-2.
[20] N. Carmona, M. Oujja, E. Rebollar, H. Römich, M. Castillejo, Analysis of corroded glasses by laser induced breakdown spectroscopy, Spectrochim. Acta B 60 (2005) 1155–1162, https://doi.org/10.1016/j.sab.2005.05.016.
[21] S. Klein, T. Stratoudaki, V. Zafiropulos, J. Hildenhagen, K. Dickmann, T. Lehmkuhl,

Laser-induced breakdown spectroscopy for on-line control of laser cleaning of sandstone and stained glass, Appl. Phys. A 69 (1999) 441–444, https://doi.org/10.1007/s003399900102.
[22] S. Klein, J. Hildenhagen, K. Dickmann, T. Stratoudaki, V. Zafiropulos, LIBS spectroscopy for monitoring and control of the laser cleaning process of stone and medieval glass, J. Cult. Herit. 1 (2000) S287–S292, https://doi.org/10.1016/S1296-2074(00)00173-4.
[23] K. Müller, H. Stege, Evaluation of the analytical potential of laser-induced breakdown spectroscopy (LIBS) for the analysis of historical glasses, Archaeometry 45 (2003) 421–433, https://doi.org/10.1111/1475-4754.00119.
[24] C.M. Bridge, J. Powell, K.L. Steele, M.E. Sigman, Forensic comparative glass analysis by laser-induced breakdown spectroscopy, Spectrochim. Acta B 62 (2007) 1419–1425, https://doi.org/10.1016/j.sab.2007.10.015.
[25] C. Barnett, E. Cahoon, J.R. Almirall, Wavelength dependence on the elemental analysis of glass by laser induced breakdown spectroscopy, Spectrochim. Acta B 63 (2008) 1016–1023, https://doi.org/10.1016/j.sab.2008.07.002.
[26] E.M. Rodriguez-Celis, I.B. Gornushkin, U.M. Heitmann, J.R. Almirall, B.W. Smith, J.D. Winefordner, N. Omenetto, Laser-induced breakdown spectroscopy as a tool for discrimination of glass for forensic applications, Anal. Bioanal. Chem. 391 (2008) 1961–1968, https://doi.org/10.1007/s00216-008-2104-y.
[27] J.-I. Yun, R. Klenze, J.-I. Kim, Laser-induced breakdown spectroscopy for the on-line multielement analysis of highly radioactive glass melt simulants. Part II: analyses of molten glass samples, Appl. Spectrosc. 56 (2002) 852–858, https://doi.org/10.1366/000370202760171518.
[28] E.C. Jung, D.H. Lee, J.-I. Yun, J.G. Kim, J.W. Yeon, K. Song, Quantitative determination of uraniumand europiumin glassmatrix by laser-induced breakdown spectroscopy, Spectrochim. Acta B 66 (2011) 761–764, https://doi.org/10.1016/j.sab.2011.09.002.
[29] I. Choi, G.C.Y. Chan, X. Mao, D.L. Perry, R.E. Russo, Line selection and parameter optimization for trace analysis of uranium in glass matrices by laser-induced breakdown spectroscopy (LIBS), Appl. Spectrosc. 67 (2013) 1275–1284, https://doi.org/10.1366/13-07066.
[30] C. Gerhard, J. Hermann, L. Mercadier, L. Loewenthal, E. Axente, C.R. Luculescu, T. Sarnet, M. Sentis, W. Viöl, Quantitative analyses of glass via laser-induced breakdown spectroscopy in argon, Spectrochim. Acta B 101 (2014) 32–45, https://doi.org/10.1016/j.sab.2014.07.014.
[31] J. Hermann, E. Axente, F. Pelascini, V. Craciun, Analysis of multielemental thin films via calibration-free laser-induced breakdown spectroscopy, Anal. Chem. 91 (2019) 2544–2550, https://doi.org/10.1021/acs.analchem.8b05780.
[32] C.-T. Chen, D. Banaru, T. Sarnet, J. Hermann, Two-step procedure for trace element analysis in food via calibration-free laser-induced breakdown spectroscopy, Spectrochim. Acta B 150 (2018) 77–85, https://doi.org/10.1016/j.sab.2018.10.011.
[33] A. Husakou, J. Herrmann, Supercontinuum generation in photonic crystal fibers made from highly nonlinear glasses, Appl. Phys. B 77 (2003) 227–234, https://doi.org/10.1007/s00340-003-1227-2.
[34] V.L. Kalashnikov, E. Sorokin, I.T. Sorokina, Raman effects in the infrared supercontinuum generation in soft-glass PCFs, Appl. Phys. B 87 (2007) 37–44, https://doi.org/10.1007/s00340-006-2545-y.
[35] J. Hermann, L. Mercadier, E. Mothe, G. Socol, P. Alloncle, On the stoechiometry of mass transfer from solid to plasma during pulsed laser ablation of brass, Spectrochim. Acta B 65 (2010) 636–641, https://doi.org/10.1016/j.sab.2010.03.015.
[36] J. Hermann, D. Grojo, E. Axente, C. Gerhard, M. Burger, V. Craciun, Ideal radiation source for plasma spectroscopy generated by laser ablation, 053210 1-6, Phys. Rev. E 96 (2017), https://doi.org/10.1103/PhysRevE.96.053210.
[37] R. McWhirter, Spectral intensities, in: R.H. Huddleston (Ed.), Plasma Diagnostic Techniques, Academic, New York, 1965, pp. 201–264.
[38] M. Cirisan, M. Cvejić, M.R. Gavrilović, S. Jovicević, N. Konjević, J. Hermann, Stark broadening of Al II lines in a laser-induced plasma, J. Quant. Spectrosc. Radiat. Transfer. 133 (2014) 652–662, https://doi.org/10.1016/j.jqsrt.2013.10.002.
[39] M. Burger, J. Hermann, Stark broadening measurements in plasmas produced by laser ablation of hydrogen containing compounds, Spectrochim. Acta B 122 (2016) 118–126, https://doi.org/10.1016/j.sab.2016.06.005.
[40] D.R. Wood, K.L. Andrew, Arc Spectrum of Lead, J. Opt. Soc. Am. 58 (1968) 818–829, https://doi.org/10.1364/JOSA.58.000818.
[41] C.E. Moore, Selected Tables of Atomic Spectra, Atomic Energy Levels and Multiplet Tables – O I, in: Nat. Stand. Ref. Data Ser., NSRDS-NBS 3 (Sect. 7), 33 pp. (Nat. Bur. Stand., U.S., 1976) https://doi.org/10.6028/NBS.NSRDS.3sec7.
[42] L.J. Radziemski, K.L. Andrew, Arc spectrum of silicon, J. Opt. Soc. Am. 55 (1965) 474–491, https://doi.org/10.1364/JOSA.55.000474.
[43] S. Falke, E. Tiemann, C. Lisdat, H. Schnatz, G. Grosche, Transition frequencies of the D lines of ^{39}K, ^{40}K, and ^{41}K measured with a femtosecond laser frequency comb, Phys. Rev. A 74 (2006) 032503, https://doi.org/10.1103/PhysRevA.74.032503.
[44] P. Juncar, J. Pinard, J. Harmon, A. Chartier, Absolute determination of the wavelengths of the sodium D_1 and D_2 lines by using a cw tunable dye laser stabilized on iodine, Metrologia 17 (1981) 77–79, https://doi.org/10.1088/0026-1394/17/3/001.
[45] H. Karlsson, U. Litzén, Revised Ba I and Ba II wavelengths and energy levels derived by Fourier transform spectroscopy, Phys. Scr. 60 (1999) 321–328, https://doi.org/10.1238/Physica.Regular.060a00321.
[46] B. Edlén, P. Risberg, The spectrum of singly-ionized calcium, Ca II, Ark. Fys. 10 (1956) 553–566.
[47] K.B.S. Eriksson, H.B.S. Isberg, The spectrum of atomic aluminium, Al I, Ark. Fys. 23 (1963) 527–542.
[48] D. Gullberg, U. Litzén, Accurate measured wavelengths of Zn I and Zn II lines of astrophysical interest, Phys. Scr. 61 (2000) 652.656, https://doi.org/10.1238/physica.regular.061a00652.
[49] W. F. Meggers, C. H. Corliss, B. F. Scribner, Tables of Spectral-Line Intensities, Part I – Arranged by Elements, Part II – Arranged by Wavelengths, Natl. Bur. Stand. Monograph 145, Nat. Bur. Stand., U.S., 600 pp. (1975). https://doi.org/10.6028/NBS.MONO.145p1.
[50] K.W. Meißner, Isotopieverschiebung im Spektrum von Magnesium Mg I, Ann. Phys. 423 (1938) 505–517, https://doi.org/10.1002/andp.19384230604.
[51] A.N. Zaidel, V.K. Prokof'ev, S.M. Raiskii, V.A. Slavnyi, E.Y. Schreider, Tables of Spectral Lines, third ed., IFI/Plenum, New York, 1970.
[52] M.M. El-Deftar, N. Speers, S. Eggins, S. Foster, J. Robertson, C. Lennard, Assessment and forensic application of laser-induced breakdown spectroscopy (LIBS) for the discrimination of Australian window glass, Forensic Sci. Int. 241 (2014) 46–54, https://doi.org/10.1016/j.forsciint.2014.04.040.
[53] G. Nave, S. Johansson, R.C.M. Learner, A.P. Thorne, J.W. Brault, A new multiplet table for Fe I, Astrophys. J., Suppl. Ser. 94 (1994) 221–459, https://doi.org/10.1086/192079.
[54] J.C. Pickering, V. Zilio, New accurate data for the spectrum of neutral silver, Eur. Phys. J. D 13 (2001) 181–185, https://doi.org/10.1007/s100530170264.
[55] A.G. Shenstone, The first spectrum of copper (Cu I), Philos. Trans. R. Soc. London, Ser. A 241 (1948) 297-322. https://doi.org/10.1098/rsta.1948.0021.
[56] F.J. Sullivan, Strontium lines in arc and solar spectra, Univ. Pittsburgh. Bull. 35 (1938) 1–8.
[57] N. Konjević, J.R. Roberts, A critical review of the Stark widths and shifts of spectral lines from non-hydrogenic atoms, J. Phys. Chem. Ref. Data 5 (1976) 209-257. https://doi.org/10.1063/1.555532.
[58] C. Fleurier, S. Sahal-Brechot, J.J. Chapelle, Stark profiles of some ion lines of alkaline earth elements, J. Quant. Spectrosc. Radiat. Transf. 17 (1977) 595–604, https://doi.org/10.1016/0022-4073(77)90019-X.
[59] N. Konjeviψ, A. Lesage, J. R. Fuhr, W. L. Wiese, Experimental Stark widths and shifts for spectral lines of neutral and ionized atoms, J. Phys. Chem. Ref. Data 31 (2002) 819-927. https://doi.org/10.1063/1.555847.
[60] Pieplow & Brandt GmbH, Product Information CERI 3000 (G/F) (2020). http://pieplow-brandt.de/en/produkte/poliermittel/ceriumoxyd-optik/ceri-3000-g-f/, 2020 (accessed 18 April 2020).
[61] K. Kato, T. Yoshioka, A. Okuwaki, Study for recycling of ceria-based glass polishing powder, Ind. Eng. Chem. Res. 39 (2000) 943–947, https://doi.org/10.1021/ie990622x.
[62] K. Binnemans, P.T. Jones, B. Blanpain, T. Van Gerven, Y. Yang, A. Walton, M. Buchert, Recycling of rare earths: a critical review, J. Clean. Prod. 51 (2013) 1–22, https://doi.org/10.1016/j.jclepro.2012.12.037.
[63] J. D. Stockham, The composition of glass furnace emissions, J. Air Pollut. Control Assoc. 21 (1971) 713-715. https://doi.org/10.1080/00022470.1971.10469588.
[64] H. Ye, Y. Li, Z. Yuan, J. Wang, Q. Xu, W. Yang, Improving UV laser damage threshold of fused silica optics by wet chemical etching technique, Proc. SPIE 9532 (2015) 953221, https://doi.org/10.1117/12.2186007.
[65] R. Catrin, J. Neauport, D. Taroux, P. Cormont, C. Maunier, S. Lambert, Magnetorheological finishing for removing surface and subsurface defects of fused silica optics, Opt. Eng. 53 (2014) 092010, https://doi.org/10.1117/1.OE.53.9.092010.
[66] Schott AG, Data sheet SF5. https://refractiveindex.info/download/data/2017/schott_2017-01-20.pdf, 2016 (accessed 18 April 2020).